

Modifying Casting Parameters to Improve the High Temperature Ductility of Investment Cast Nickel-Based Superalloy PWA 1455

A Senior Project

Presented to the Faculty of the Materials Engineering Department
California Polytechnic State University, San Luis Obispo

In Partial Fulfillment
of the Requirements for the Degree
Bachelor of Science, Materials Engineering.

by

Lars Hedin, Cole Introliigator

Advisor: Professor Blair London

Sponsor: PCC Structural, Inc.

June 2019

© 2019 Lars Hedin, Cole Introliigator

Abstract

PCC Structural, an industry leader in superalloy investment castings, has observed inconsistencies in the stress rupture performance of polycrystalline nickel-based superalloy PWA 1455. PCC has changed their casting parameters to reduce the thermal gradient during cooling but have been unable to correlate these changes with an increase in stress rupture elongation. Metallographic examination of past samples indicated microstructures composed of non-equiaxed dendritic grains with mean diameter of .021 inches along the test axis. A similar study on polycrystalline superalloys has indicated that excessive superheat temperatures above the liquidus can result in large grains identical to those observed, limiting the stress rupture ductility. Additionally, the study connected low superheats above the liquidus to an equiaxed, small grain structure. Conclusions from metallographic examination and literature review point to the necessity of lowering the pour temperature and increasing the mold temperature during casting to lessen the average grain size, promoting better stress rupture ductility. The new processing parameters produced an average grain diameter of .014 inches and resulted in sufficient stress rupture elongations, with all samples passing the minimum required by specification. Specimens with the lowest superheat temperature showed a mixed grain structure with equiaxed grains on the boundaries of the test bar and columnar grains on the interior. The observed grain morphology signals the need for additional experiments to produce a fully equiaxed structure and reach peak stress rupture performance.

Keywords: Nickel-based superalloys, nickel, based, superalloy, PWA 1455, investment casting, polycrystalline, stress rupture elongation, test specimens, property validation, casting parameters, pour temperature, mold temperature, columnar, dendrites, equiaxed grains, chill zone, process improvement, liquidus, grain structure, ductility, grain size measurement, grain morphology

Acknowledgements

We would like to thank PCC Structural (San Leandro, CA) as a whole for sponsoring and funding our senior project. Our two points of contact, Boris Luu and Julene Wagner, were incredibly helpful and responsive over the course of our project. Without their knowledge and support, our project would not have been as smooth or rewarding as it was. Additionally, we would like to thank our senior project advisor, Dr. Blair London. Professor London's casting industry experience and encouragement was extraordinarily helpful in addressing the root issue of our senior project and refining our technical communication skills. Professor Ryan Smith in the materials engineering department was also an invaluable point of contact, as his knowledge of solidification kinetics allowed for a greater understanding of our project. Lastly, we would like to thank Hajime Yamanaka for assisting us with taking quality SEM images for failure analysis.

Table of Contents

1. Introduction.....	6
1.1 Company Background.....	6
1.2 Nickel-Based Superalloys.....	6
1.2.1 Superalloy Applications.....	6
1.2.2 Processing.....	7
1.2.3 Composition.....	8
1.3 Stress Rupture Testing.....	11
1.4 Grain Structure and Ideal Performance.....	12
1.5 Summary.....	13
1.6 Problem Statement.....	14
2. Experimental Procedure.....	15
2.1 Safety.....	15
2.2 Preliminary Metallographic Analysis.....	15
2.3 Design of Experiment.....	15
2.4 Grain Size Determination.....	16
2.5 Stress Rupture Testing.....	17
2.6 Statistical Analysis.....	17
3. Results.....	18
3.1 Initial Evaluation.....	18
3.2 Stress Rupture Results from Modified Parameters.....	20
3.3 Microstructural Results.....	20
3.4 Statistical Results.....	21
3.4.1 Test for Normality Using a Normal Probability Plot.....	22
3.4.2 Two-Tailed T-test.....	23
4. Discussion.....	24
4.1 Microstructural Analysis.....	24
4.2 Stress Rupture Elongation.....	25
5. Conclusions.....	26
References.....	27

List of Figures

Figure 1. Investment cast nozzle guide vane for use in a gas turbine engine. ¹	6
Figure 2. Gas turbine engine schematic displaying different materials used depending on the temperature of the engine. ²	7
Figure 3. Ceramic shell investment casting process. ⁵	7
Figure 4. Turbine blade casting in equiaxed (a), directionally solidified (b), and single crystal (c) forms. ⁵ 8	8
Figure 5. Scanning electron image of excessive σ phase formation along the grain boundaries of superalloy RR1000. ⁶	9
Figure 6. (a) FCC crystal structure of γ phase with nickel in each face and corner. (b) Ordered crystal structure of γ' phase with nickel occupying the faces and Al, or Ti occupying the corners of the cell. ⁶ ...	10
Figure 7. Scanning electron image of γ' precipitates sheared by a dislocation pair. ⁶	10
Figure 8. Yield stress of multiple binary Ni-Al Alloys of different treatment cycles as a function of temperature. ⁶	11
Figure 9. Diagram visualizing Nabarro-Herring diffusional creep is a product of a stress gradient and resulting atom-vacancy diffusion. ⁹	12
Figure 10. Optical micrographs showing the grain size of CM 247 LC at various casting temperatures: (a) 3 thousandths at a pour temperature of 36°F above the liquidus line. (b) 6 thousandths at a pour temperature of 72°F above the liquidus line. (c) 90 thousandths at a pour temperature of 145°F above the liquidus line. ⁴	13
Figure 11. Diagram showing the cross-section (a) and longitudinal (b) cuts made on the stress rupture specimens received from PCC Structurals.....	15
Figure 12. Representative image used in grain size counting showing how the circle diameter was determined using the known length of the photographed area.	16
Figure 13. Diagram showing a stress rupture specimen pulled at elevated temperatures under a constant load until failure.	17
Figure 14. (a) Cross-section microstructure of ML. 0007385 at 50x with a stress rupture elongation of 4%. (b) Cross-section microstructure of ML. 0006897 at 50x with a stress rupture elongation of 7.5%.	18
Figure 15. Stress rupture elongation data for all previously cast samples. Yellow dots represent samples that were physically received for analysis in addition to the property data.	19
Figure 16. The stress rupture elongation was plotted alongside the average grain diameter for all seven of the material lot test bars received from PCC structurals.....	20
Figure 17. The average grain diameter (a) and stress rupture elongation (b) of each standard casting parameter datapoint was plotted alongside the relative z-scores and compared to a linear regression.	22
Figure 18. The average grain diameter (a) and stress rupture elongation (b) of each changed casting parameter datapoint was plotted alongside the relative z-scores and compared to a linear regression.	23
Figure 19. Scanning electron images of the stress rupture fracture surface of ML. 0007359. (a) Superficial fracture surface at 46x. (b) Large columnar dendrite impression at 110x. (c) Shrinkage pores within the dendrite impression circled in red at 347x.	24

Figure 20. Stress rupture elongation and grain diameter of all specimens examined (standard and changed casting parameters). 25

List of Tables

Table I. Composition of Common Commercial Nickel-Based Superalloys (bal. wt. % Ni) ²	8
Table II. Stress Rupture Test Results of CM 247 LC superalloy at 1800°F/ 29 ksi ⁴	13
Table III. Modified Casting Parameter Matrix	16
Table IV. Longitudinal Cross-sections of Material Lots Cast with PCC Standard Parameters.....	18
Table V. Modified Casting Parameter Matrix with Resulting Stress Rupture Elongations	20
Table VI. Comparative Microstructures of All Modified Casting Parameters Combinations.....	21
Table VII. Mean and Standard Deviation of Stress Rupture Elongation and Grain Size	22
Table VIII. Outputs from T-Test Comparing Standard and Modified Casting Procedures.....	23

1. Introduction

1.1 Company Background

PCC Structural (San Leandro, CA) is a global leader in investment castings for use in the aerospace industry. Structural components are made from metallic families of aluminum, titanium, and nickel-based superalloys. PCC supplies precision castings to additional industries such as medical prothesis and military armaments. Typical cast nickel-based parts produced by PCC include turbine blades and nozzle guide vanes (Figure 1).

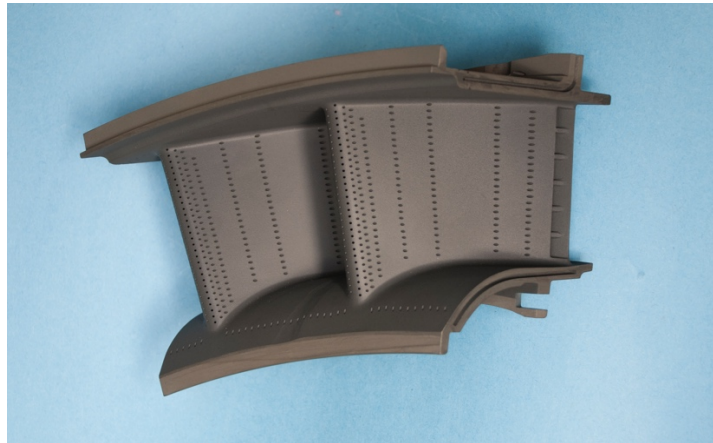


Figure 1. Investment cast nozzle guide vane for use in a gas turbine engine.¹

Cast aerospace components require extensive property validation as any unexpected failure will have catastrophic effects on the aircraft. While the investment casting process is highly refined, certain alloys or parts sometimes yield mechanical properties that are out of specification, requiring additional work both by metallurgists and process engineers. This project is focused on understanding the processing of a particular alloy and how the properties can be improved through design of experiment, testing, and analysis.

1.2 Nickel-Based Superalloys

1.2.1 Superalloy Applications

Nickel-based superalloys have been a vital component to the success of gas turbine engines since their emergence in the 1940s. This family of metals is known for high temperature strength, high elongation before failure, and resistance to oxidation in extreme environments.² The unique combination of properties found within this class of materials is paramount to the technological advancement of aircraft engine components. Additionally, the castability of these alloys maximizes their potential as their distinctive mechanical and creep properties can be applied in complex part geometries. Nickel-based superalloys typically comprise up to 50% of the total gas turbine engine weight, being utilized primarily in the later sections of the engine (Figure 2). After the initial intake of air, combustion of jet fuel can result in service temperatures of over 1500°F. Only through advanced manufacturing and treatment methods can superalloys consistently perform in these extreme environments. Highly advanced alloys and refined forming

techniques have enabled this family of metals continuously push the limits of turbine engine technology.

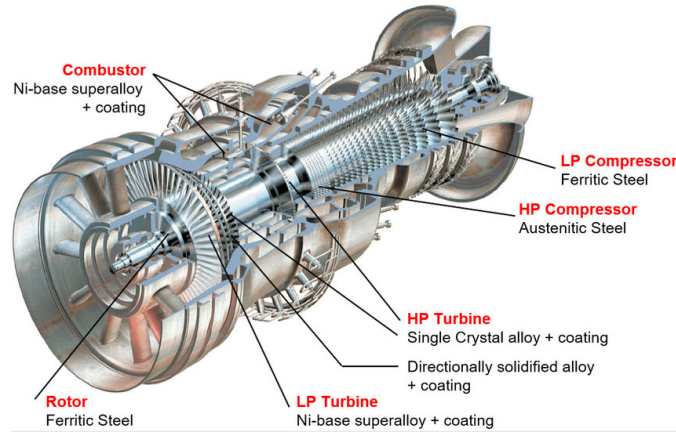


Figure 2. Gas turbine engine schematic displaying different materials used depending on the temperature of the engine.²

1.2.2 Processing

Investment casting serves as the major shaping process for most superalloys as it results in superior high temperature mechanical properties when compared to forged components.² Complex part geometries are formed by a ceramic shell in which the molten metal is poured in and processed in stem-like batches (Figure 3). Prior to pouring, a wax replica of the part is coated in a ceramic slurry before being evaporated in a low temperature heat treatment. After solidification of the metal within the mold, the ceramic outer-layer is chipped off and the parts are sent to post processing and finishing. Most superalloys melt at temperatures above 2000°F, where oxidation and contamination of the metal becomes an issue. To combat this problem, the metal is poured in a vacuum to minimize any potential impurities.⁴ The lack of oxygen enables the material to be heated to extreme temperatures without reacting with the atmosphere, reducing the possibility of premature failure.

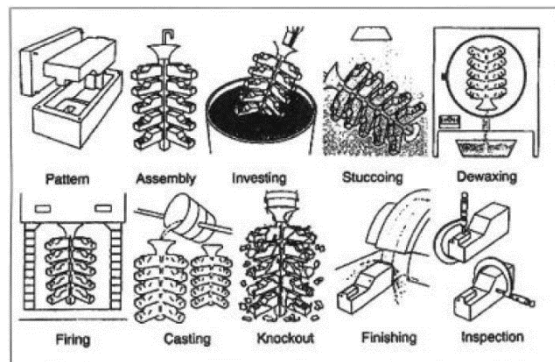


Figure 3. Ceramic shell investment casting process.⁵

As gas turbine engines have become more thermally efficient, their improved performance proportionally subjects their components to increasingly harsher environments. This pushed superalloy manufacturers to find new ways to improve high temperature properties, leading to

the development of directionally solidified and eventually single crystal components.⁶ Compared to conventional casting, directional solidification aligns the grains in the direction of intended loading, improving the high temperature properties significantly. Single crystal superalloys take this a step further, removing grains entirely and thus eliminating the issues that arise with polycrystalline materials (Figure 4). Currently, single crystal alloys are used for components that experience the most extreme temperatures from combustion under the highest loads, as they exhibit superior creep and corrosion properties. Directionally solidified and polycrystalline castings still are used in cooler regions of turbine engines due to lower cost and ease of manufacturing.

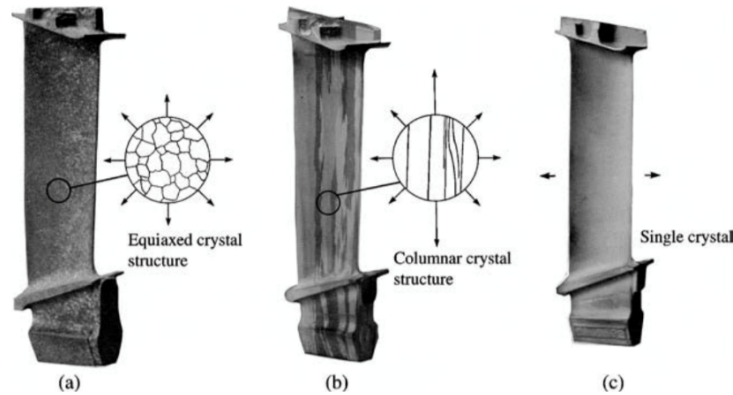


Figure 4. Turbine blade casting in equiaxed (a), directionally solidified (b), and single crystal (c) forms.⁵

1.2.3 Composition

Although mainly comprised of nickel, superalloys can contain up to 40-50 wt. % of 5-10 alloying elements serving a multitude of purposes (Table I). These additions assist in the formation of grain boundary carbides, formation and strengthening of precipitates, and improvements in corrosion behavior.

Table I. Composition of Common Commercial Nickel-Based Superalloys (bal. wt. % Ni)²

Alloy	Cr	Co	Mo	W	Ta	Re	Nb	Al	Ti	Hf	C	B	Y	Zr	
<i>Conventionally Cast Alloys</i>															
Mar-M246	8.3	10.0	0.7	10.0	3.0	—	—	5.5	1.0	1.50	0.14	0.02	—	0.05	
Rene' 80	14.0	9.5	4.0	4.0	—	—	—	3.0	5.0	—	0.17	0.02	—	0.03	
IN-713LC	12.0	—	4.5	—	—	—	2.0	5.9	0.6	—	0.05	0.01	—	0.10	
CI023	15.5	10.0	8.5	—	—	—	—	4.2	3.6	—	0.16	0.01	—	—	
<i>Directionally Solidified Alloys</i>															
IN792	12.6	9.0	1.9	4.3	4.3	—	—	3.4	4.0	1.00	0.09	0.02	—	0.06	
GTD111	14.0	9.5	1.5	3.8	2.8	—	—	3.0	4.9	—	0.10	0.01	—	—	
<i>First-Generation Single-Crystal Alloys</i>															
PWA 1480	10.0	5.0	—	4.0	12.0	—	—	5.0	1.5	—	—	—	—	—	
Rene' N4	9.8	7.5	1.5	6.0	4.8	—	0.5	4.2	3.5	0.15	0.05	0.00	—	—	
CMSX-3	8.0	5.0	0.6	8.0	6.0	—	—	5.6	1.0	0.10	—	—	—	—	

Carbon exhibits a high affinity to bond with heavy elements such as Hf, Ti, W, Mo, and V, which form carbides that migrate to the grain boundaries (Figure 5). Carbides tend to form as MC and are transformed through heat treatment into $M_{23}C_6$, M_6C , and M_7C_3 . High temperature exposure during service can also cause this transformation, consolidating the heavy elements into larger, interconnected carbides.² While these compounds can serve as crack initiation sites during

fatigue, their presence is essential in preventing grain boundary sliding and diffusion during high temperature service. The large, blocky formations are able to pin boundaries, preventing movement and improving rupture properties.

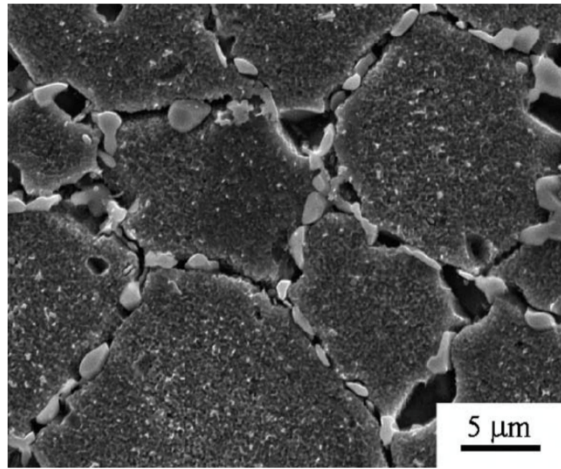


Figure 5. Scanning electron image of excessive σ phase formation along the grain boundaries of superalloy RR1000.⁶

Resistance to oxidation during use is achieved through alloying elements that form a strong, protective oxide-layer. Similar to stainless steel, Cr is added to many superalloys to promote the formation of an exterior layer that prevents oxidation during use.² Superalloys contain a myriad of elements serving different purposes. Therefore, unintended compounds can sometimes form, which adversely affect the intended properties. Low melting point elements such as Pb, Bi, Ag, and S at impurity levels can cause significant detriment to both the mechanical and corrosion resistant properties that are pivotal to the use of superalloys. Sulfur can significantly affect corrosion resistance of superalloys by compromising the bonding between the oxide scale and the bulk metal.⁶ The high solubility of sulfur within the oxide scale diminishes the strength of Van der Waal forces on the surface, causing the protective layer to flake off and continuously expose unoxidized raw material. To combat sulfur impurities, manufacturers coat crucibles with protective linings with the addition of rare earth alloying elements to form stable sulfuric compounds. These techniques have been shown to be effective at keeping sulfur levels below 10 ppm in most conventional vacuum cast products.⁶

Superalloys achieve many of their desirable high temperature properties due to reactions that occur in the nickel-aluminum system. Through controlled solidification and subsequent heat treatments, intermetallic compounds of nickel and aluminum will precipitate into a second phase within the nickel lattice. The primary γ phase is a solid solution nickel phase that includes Co, Cr, and Mo as stabilizers. The secondary phase, γ' , is an ordered phase comprised of the compound Ni_3Al (Figure 6).

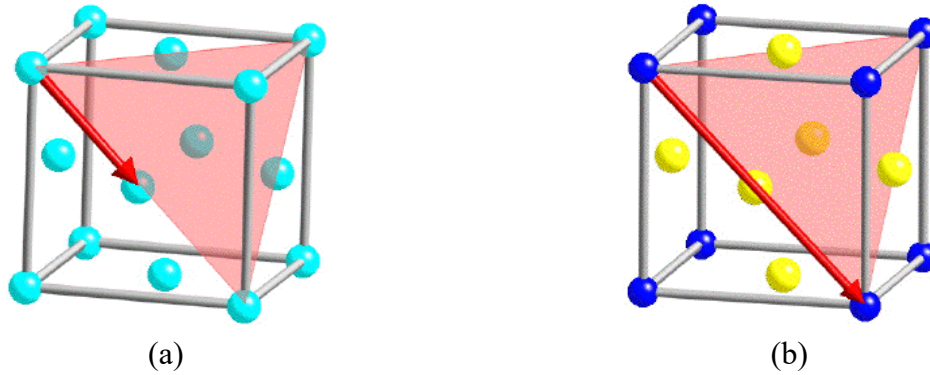


Figure 6. (a) FCC crystal structure of γ phase with nickel in each face and corner. (b) Ordered crystal structure of γ' phase with nickel occupying the faces and Al, or Ti occupying the corners of the cell.⁶

The ordered regions are aligned with the planes of the parent phase, resulting in coherent strain within the matrix and impeding the movement of dislocations even at high temperatures close to T_m .⁶ The formation and strengthening of this phase is aided by elements Ti, Ta, and Nb. While the chemical composition is partially responsible for the structure of γ' , casting parameters dictating cooling rate have significant impact, affecting the size of the secondary phase.² A fast cooling rate ($\sim 40\text{K/min}$) typically results in a unimodal, medium sized precipitates, while slower cooling rates can produce populations of either small or large compounds. The boundary between the γ' and γ phases is responsible for the elevated temperature strength and high resistance to plastic deformation of nickel-based superalloys. The misfit strain of this boundary serves as the mechanism of stopping dislocations in nickel superalloys, which is not reduced at high temperatures because of the high stability of the ordered Ni_3Al phase. The mechanism that impedes dislocation movement through the nickel lattice is that dislocations must move in pairs through the γ'/γ boundary to prevent the formation of high energy anti-phase boundaries between the two phases in certain crystallographic slip systems (e.g. $a/2\langle 110 \rangle \{111\}$) (Figure 7). Gamma-prime precipitate sizing and volume fraction will affect this mechanism, where smaller precipitates have less of a strengthening effect than large, closely spaced ones.

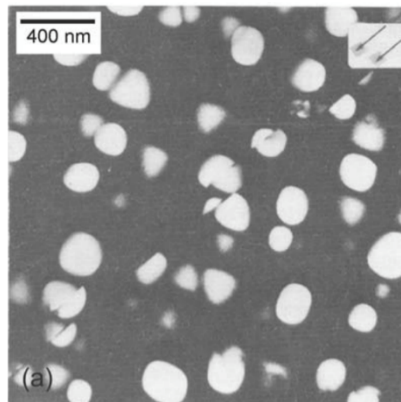


Figure 7. Scanning electron image of γ' precipitates sheared by a dislocation pair.⁶

The low temperature dependence of yield strength within precipitate strengthened superalloys can be explained by the stability of the γ' phase within the lattice of γ . In one study, the sizing of

the precipitates in a binary Ni-Al system was compared to the yield strength at different temperatures (Figure 8). It is apparent that the solid solution nickel compound has significantly lower strength than the aged compound and drops off a fair amount as the temperature increases. The precipitation strengthened alloys (Ni- 14 at% Al) all show superior strength, but only the alloy that received the heat treatment producing optimal γ' phase size was able to show minimal decrease in yield strength as a function of temperature. While room temperature tensile properties are enormously important in superalloy applications, their true value lies in their ability to withstand cyclic loading at extreme temperatures and exhibit resistance to stress rupture.

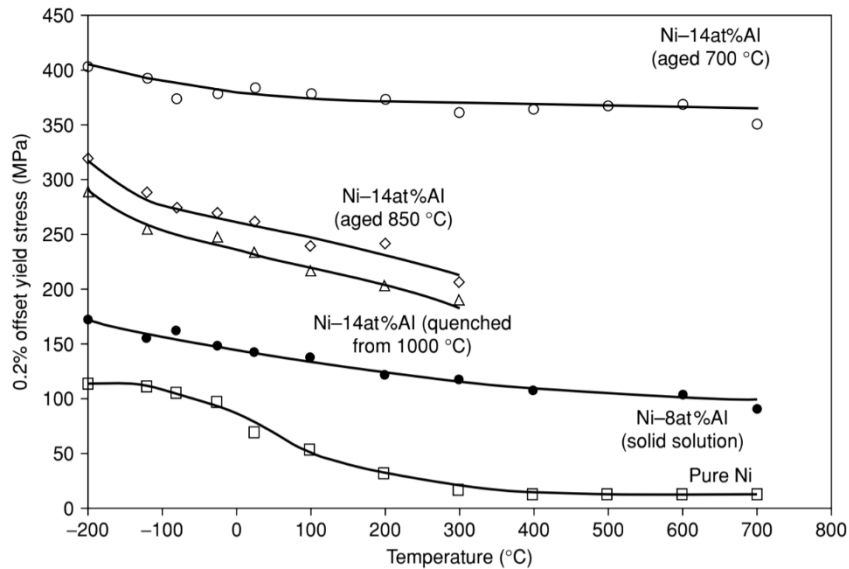


Figure 8. Yield stress of multiple binary Ni-Al Alloys of different treatment cycles as a function of temperature.⁶

1.3 Stress Rupture Testing

Stress rupture testing is important in measuring the performance of nickel-based superalloys as it simulates the conditions experienced in application. A stress rupture test applies a static load at a constant temperature to a test bar usually 70 to 80% of the melting temperature of the metal.⁷ The test piece is pulled until failure producing values of time until failure (hours) and the percent elongation. While the property relies heavily on the volume fraction of γ' , the grain size and structure of conventionally cast products have a major influence on the mechanical properties as well. Polycrystalline or equiaxed grain structures have been found to be more susceptible to failure by cracking along grain boundaries at elevated temperatures.⁸

This failure mechanism has been partially mitigated by the production of directionally solidified and single crystal parts as they have few to no grain boundaries. However, cost and ease of manufacturing encourage greater control of equiaxed grain formation in parts. This control stems from understanding Nabarro-Herring diffusion creep that occurs during stress rupture testing. Nabarro-Herring creep occurs at relatively high temperatures and low stresses and is noted for the flow of vacancies through the grains. As the tensile load is applied to the test bar, the grains in that axis are put in tension with the other sides in compression. At the elevated temperature of

the test, the grains in tension become sources of vacancies while the grains in compression become vacancy sinks.⁹ A vacancy flux forms through the bulk of the grain, leading to a critical accumulation of vacancies at the compressed grains and eventual failure due to grain separation and grain boundary sliding (Figure 9). The strain rate of Nabarro-Herring creep is moderately affected by grain size, since a fine-grained structure will result in a high strain rate and shorten the stress rupture life of the part. Thus, larger coarse grains of 3 to 6 thousandths of an inch are comparatively favored to provide adequate space for vacancies to collect before failure.⁶

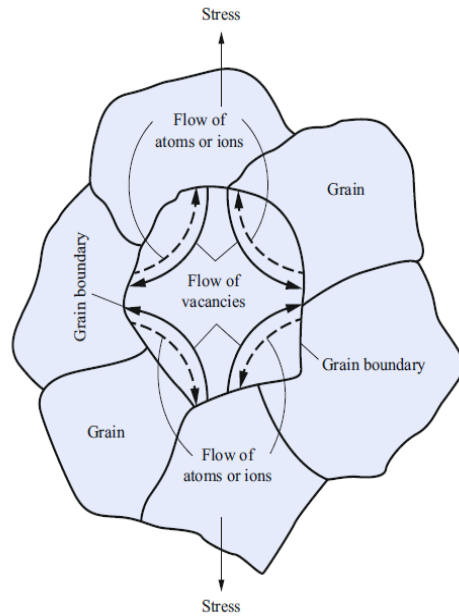


Figure 9. Diagram visualizing Nabarro-Herring diffusional creep is a product of a stress gradient and resulting atom-vacancy diffusion.⁹

1.4 Grain Structure and Ideal Performance

The desired grain structure and size of nickel-based superalloy castings have been shown to be achieved by controlling the superheating of the alloy before pouring. A study on polycrystalline nickel-based superalloy CM 247 LC has shown that superheats of 36°F to 144°F above the liquidus line will yield coarse equiaxed grains of 3 to 6 thousandths of an inch, while superheats ranging from 145°F and above yield columnar dendrites of 90 thousandths in length (Figure 10).

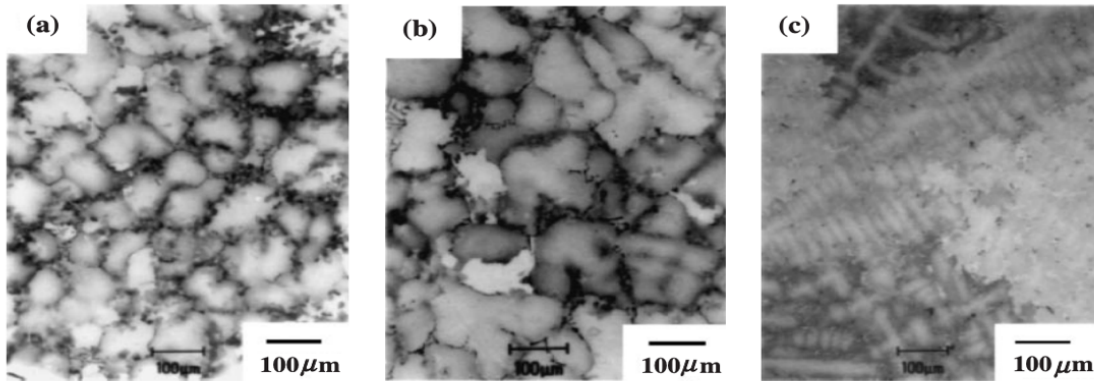


Figure 10. Optical micrographs showing the grain size of CM 247 LC at various casting temperatures: (a) 3 thousandths at a pour temperature of 36°F above the liquidus line. (b) 6 thousandths at a pour temperature of 72°F above the liquidus line. (c) 90 thousandths at a pour temperature of 145°F above the liquidus line.⁴

The columnar to equiaxed transition increased the percent elongation of CM 247 LC by a factor of 1.3-1.5 from the 9×10^{-2} grains while maintaining an excellent creep life relative to its pertinent specification (Table II). The grain morphology transition and its effect on the stress rupture elongation seen in this study has yet to be observed in other polycrystalline nickel-based superalloys. However, considering the compositional similarities of polycrystalline superalloys (Table I), the study serves as a baseline reference to improve the performance of similar alloys and ensure their continued use in industry.

Table II. Stress Rupture Test Results of CM 247 LC superalloy at 1800°F/ 29 ksi⁴

Temperature above Liquidus Line (°F)	Grain size (inches)	Creep life (h)	Stress Rupture Elongation (%)
36-71°F	3×10^{-3}	47	9
72-144°F	6×10^{-3}	69	8
145°F+	9×10^{-2}	102	6

1.5 Summary

The casting process of nickel superalloys has been refined over the past decades to move from conventionally cast to directionally solidified, which grows the grains in the direction of intended stress. Additionally, generations of single crystal superalloy development have removed the problems posing polycrystalline structures altogether, each type making greater improvements in the alloy service temperature, tensile properties, and failure life.⁶ Conventionally cast alloys with equiaxed grain structures are still primarily used in relatively cooler parts of the engine due to cost of alloy and ease of production when compared to their single crystal counterparts.² In continuing development of single crystal superalloys, the problems affecting conventionally cast alloys persist. Pratt and Whitney designed nickel-based superalloy PWA 663 for the express purpose of having an alloy exhibit high strength at high temperatures (1900°F) with a creep elongation above 1% at 1400°F. Other nickel-based superalloys typically became embrittled at the latter temperature; thus, PWA 663 was an upgrade from other nickel-based superalloys at the

time.¹⁰ Hafnium was later added to PWA 663 and showed significant improvement in creep ductility at 1400°F and thermal fatigue resistance, resulting in the alloy PWA 1455. The hafnium additions partition to the grain boundaries of the alloy through its processing. The resulting carbides ultimately strengthen and limit diffusional creep along the boundaries.⁶ However, these additions have not been linked to similar benefits at higher temperatures (1800°F). Stress rupture life at 1800°F and 24.5 ksi ranged from 34 to 66 hours, but changes to PWA 1455's composition and PCC Structural's internal qualification requirements for testing at a higher creep load (29 ksi) pose new challenges in qualifying it for further use in turbofan blade linings and casings.¹⁰

1.6 Problem Statement

PCC Structural's has observed inconsistencies in the stress rupture elongation performance of nickel-based superalloy PWA 1455. Modifications to the investment casting procedures may improve the test bar stress rupture elongation to consistently meet material specifications, reducing the frequency of re-tests and scrapped parts. As nickel-based superalloys are expensive to process, reducing waste material has significant economic incentive. Thus, multiple changes were made to the investment casting parameters of pour and mold temperatures to change the grain morphology of the test bars. These experimental parameters may prove the concept of the grain size and related stress rupture elongation performance of nickel-based superalloy PWA 1455 is dependent on the superheat temperature of the castings.

2. Experimental Procedure

2.1 Safety

Standard lab safety was followed over the course of this project, including personal protective equipment, proper chemical storage, and safe lab practices. A standard operating procedure was written for the use of metallographic etchant, which was used with proper etching procedure. In rough preparation of samples, all pertinent standard operating procedures were followed in the mounting of specimens used in this project.

2.2 Preliminary Metallographic Analysis

To determine the microstructure and gain insight into the effects of the processing parameters on PWA 1455, several cast specimens poured with the PCC's standard parameters were received for examination. These bars were as-cast samples that had not yet been machined for stress rupture testing. This allowed for the viewing of the entire microstructure without any areas cut off, allowing for a better representation of casting parameter influence on the structure. The samples were viewed both longitudinally and cross sectionally (Figure 11). Each specimen was cut using the same sequence, where a small piece was cut off for cross-sectional viewing before making the second cut to produce a longitudinal piece.



Figure 11. Diagram showing the cross-section (a) and longitudinal (b) cuts made on the stress rupture specimens received from PCC Structurals.

After cutting the test bars into viewable components, rough preparation and polishing were conducted using silicon carbide grinding paper and diamond abrasive polishing pads, allowing the samples to be etched. Diamond abrasives ranging from 6 to 1 micrometer were utilized before performing the etch. The etchant used was 2mL of 30% H_2O_2 and 50 mL of 70% hydrochloric acid to show the grain boundaries and precipitates. As suggested by PCC Structurals, the samples were immersion etched for 10-15 seconds to show significant contrast between grains of different orientations.





Preliminary metallographic analysis was conducted on all of the test bars produced using the standard casting parameters. The same rough preparation and etching procedures were used for metallographic examination of the castings later received produced using changed casting parameters. This allowed the same area in the test bars to be viewed each time etched using the same procedure, which reduced uncertainty in the data.

2.3 Design of Experiment

Two pour temperatures and two preheat mold temperatures were proposed to potentially achieve consistent stress rupture elongation and an equiaxed grain structure in the test bars (Table III).

These temperatures were also chosen to allow PCC to have complete fill throughout the mold upon casting.

Table III. Modified Casting Parameter Matrix

		Pour Temperature	
		2500°F	2600°F
Mold Temperature	2000°F		
	2100°F		

Test bars were poured in PCC’s standard lost wax investment casting rig and remained unmachined after cooling. The bars were sent to Element Testing (Huntington Beach, CA) for stress rupture testing at 1800°F and 29 ksi. Two bars were reserved from each casting parameter lot for metallographic evaluation.

2.4 Grain Size Determination

Average grain diameter was found on the longitudinal section for samples as this axis was aligned with the load during stress rupture testing. The grain size was evaluated using ASTM standard E112 for standard grain size measurement, with a magnification of 50x.¹¹ Due to the not-fully equiaxed structure of the grains, the circle method was used to count intersections as dictated by specification. The circumference of the circle was determined using known length of each photo (Figure 12). The length of each photo was found by using a calibrated marker bar to measure the length in pixels before conversion to inches.

To determine the average grain diameter, the circumference of the circle was divided by the number of intersections. Circle intersections for each sample were counted multiple times by two different individuals to ensure reduce bias and possible error.

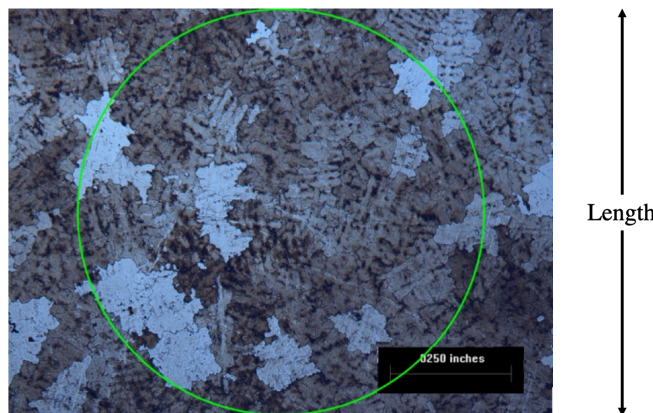


Figure 12. Representative image used in grain size counting showing how the circle diameter was determined using the known length of the photographed area.

2.5 Stress Rupture Testing

In order to simulate the conditions experienced by nickel-based superalloys in a gas turbine engine, a unique mechanical test is used in which a fixed load is applied to a specimen at a constant temperature until fracture (Figure 13). As dictated by specification PWA 1455, the specimens were pulled at 1800°F and 29 ksi. The output parameters are elongation and time at break, with the specification dictating minimums of 5.5% and 23 hours respectively.

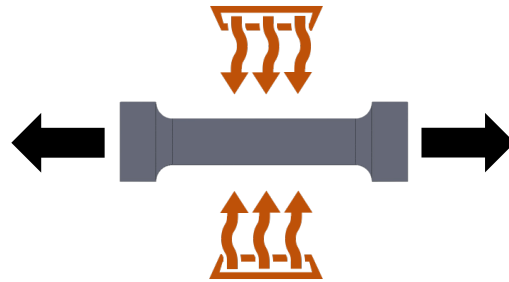


Figure 13. Diagram showing a stress rupture specimen pulled at elevated temperatures under a constant load until failure.

2.6 Statistical Analysis

To quantify the differences between the two groups of prior casting parameters and changed casting parameters, statistical tests were utilized. First, all datasets were assessed for relative normality so that tests could be run. This was done by using a normal probability plot by determining the deviation of each data point from a linear regression line. All samples passed the test for normality. It was assumed that the distributions have relatively equal variance as the sample size was the same for all compared groups.

A two tailed t-test was used for comparison as a two tailed test assumes that the groups could vary in either direction which is slightly more conservative. The two groups compared were the samples with standard casting parameters and the samples with altered casting parameters. The variables tested were the stress rupture elongation and grain diameter.

3. Results

3.1 Initial Evaluation

Metallography was performed on the seven received samples in attempt to form a connection between grain diameter and stress rupture properties. The microstructures were imaged in dark field and converted to grayscale to highlight the contrast between grain orientations. All of the sample cross sections showed large columnar dendrites extending toward the center of the specimens. There was no evidence of an equiaxed zone in the center of the test specimen. Test bars from material lots (ML) 0007385 and 0006897 showed similar microstructures with stress rupture elongations of 4% and 7.5% respectively. There was no indication of a relationship between grain size and high temperature ductility (Figure 14).

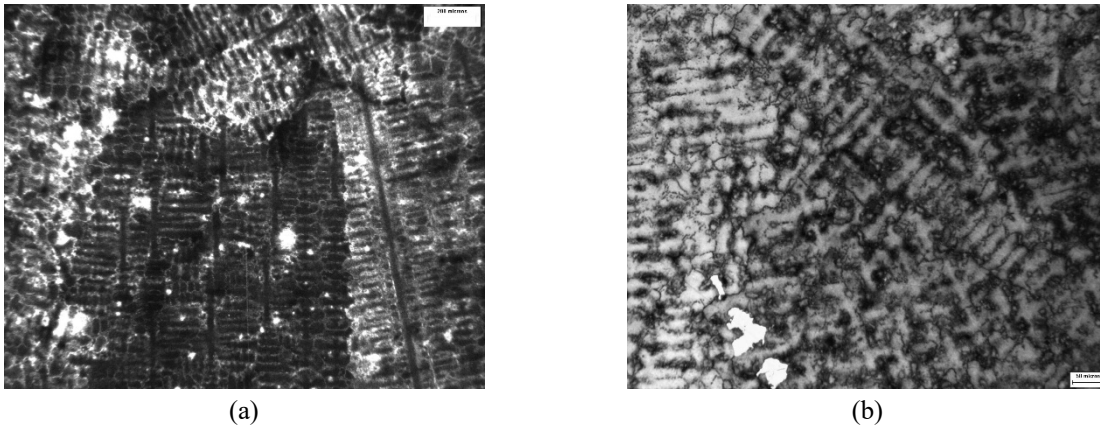


Figure 14. (a) Cross-section microstructure of ML. 0007385 at 50x with a stress rupture elongation of 4%. (b) Cross-section microstructure of ML. 0006897 at 50x with a stress rupture elongation of 7.5%.

The longitudinal cross sections of the received samples showed no columnar dendrites, but large randomly shaped grains averaging 21 thousandths of an inch (Table IV).

Table IV. Longitudinal Cross-sections of Material Lots Cast with PCC Standard Parameters

ML. 0006897	ML. 0007105	ML. 0007385	ML. 0007359-01
ML. 0007359-02	ML. 0007765	ML. 0007974	

The stress rupture results from test bars processed using PCC’s standard parameters showed a wide spread of stress rupture elongations. As seen in Figure 15, over the past two years, 26 orders of castings poured using PWA 1455 showed 4 random inadequate stress rupture elongation failures as indicated by the red line. All stress rupture results are ordered chronologically, with the most recent samples on the left. Out of the 26 material lots, 7 of them had spare test bars which were supplied for analysis by PCC Structurals. The received test specimens are highlighted in yellow. It is assumed that the microstructures and properties observed in the received samples are representative of the entire group, as they possess a varying performance range similar to all of the reported stress rupture elongation values.

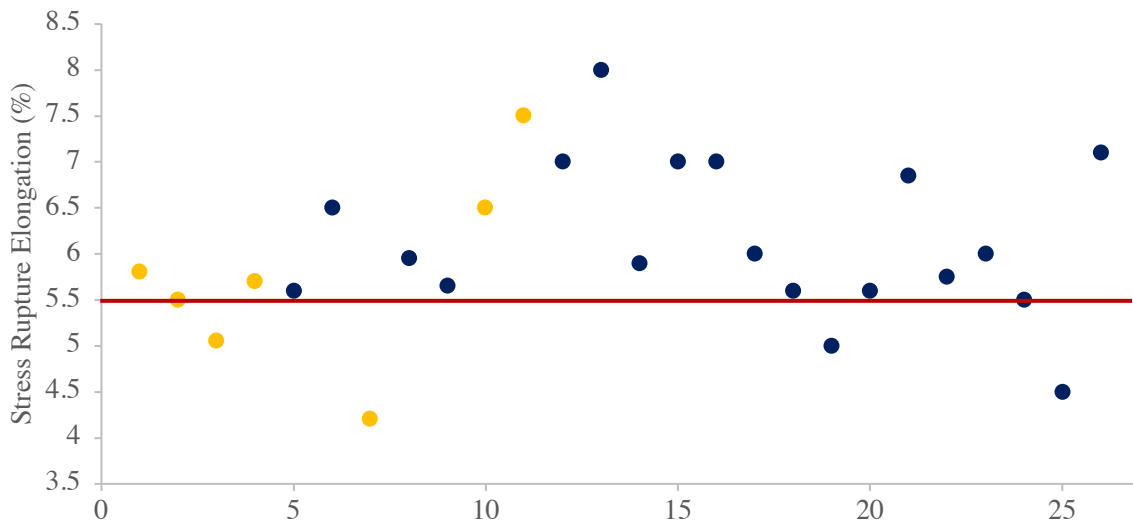


Figure 15. Stress rupture elongation data for all previously cast samples. Yellow dots represent samples that were physically received for analysis in addition to the property data.

Grain size measurements from all seven specimens received from PCC are displayed in Figure 16, where stress rupture elongation is also plotted. Various trendlines including linear and polynomial were applied in attempt to quantify a relationship between the two parameters, but they appeared to be unrelated. The elongation that the samples would fail at appeared to have no correlation to the grain size. The average stress rupture elongation was 5.75 % with a standard deviation of 1.04 %, while the average grain diameter was 21.1 thousandths of an inch with a standard deviation of 3.68 thousandths of an inch.

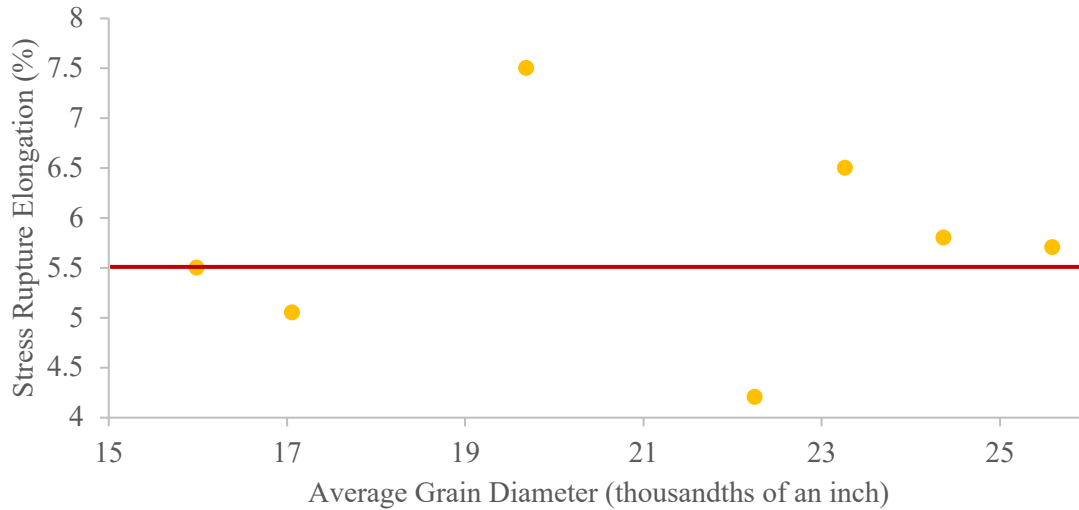


Figure 16. The stress rupture elongation was plotted alongside the average grain diameter for all seven of the material lot test bars received from PCC Structurals.

3.2 Stress Rupture Results from Modified Parameters

All test bars manufactured with modified casting parameters met or exceed the minimum stress rupture requirement of 5.5% (Table V). Samples 1 and 2 cast with a pour temperature of 2500°F and a mold temperature of 2000°F reported elongations of 5.7% and 5.5% respectively. Samples 5 cast with a pour temperature of 2500°F and a mold temperature of 2100°F reported an elongation of 5.6%, while sample 6 cast with the same parameters reported the highest elongation of the lot at 7.1%. Samples 3 and 4 cast with a pour temperature of 2600°F and a mold temperature of 2000°F reported elongations of 5.6% and 5.5% respectively as well. Samples 7 cast with a pour temperature of 2600°F and a mold temperature of 2100°F reported the second highest elongation of the lot at 6.4%, while sample 8 reported a 5.6% elongation at the same casting parameters.

Table V. Modified Casting Parameter Matrix with Resulting Stress Rupture Elongations

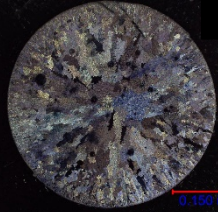
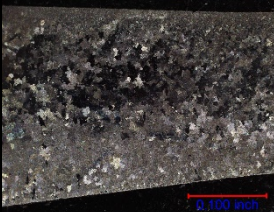
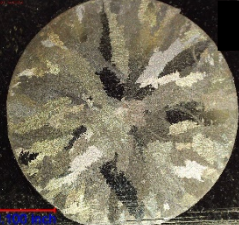


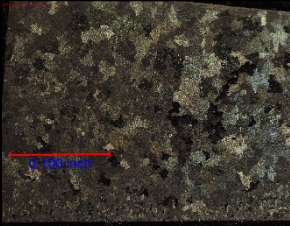

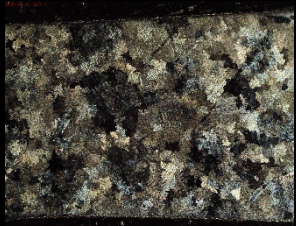
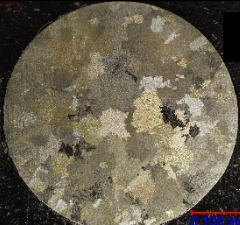

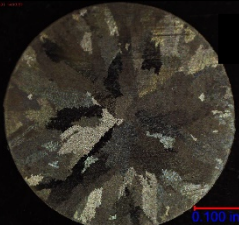


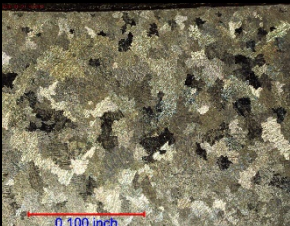


		Pour Temperature			
		2500°F		2600°F	
Mold Temperature	2000°F	5.7% S1	5.5% S2	5.6% S3	5.5% S4
	2100°F	5.6% S5	7.1% S6	6.4% S7	5.6% S8

3.3 Microstructural Results

A pour temperature 125°F above the liquidus (2500°F) did not produce a coarse grained equiaxed microstructure as expected. As seen in Table VI, a chill zone is seen on the border of all samples with a pour temperature of 2500°F with large non-equiaxed grains occupying the

center of the cross and longitudinal sections. Samples 3 and 4 cast at 2600°F and 2000°F showed large columnar dendrites extending into the cross-sections of their microstructures. Their longitudinal sections showed similar non-equiaxed grains across the face. Samples 7 and 8 cast with a pour temperature of 2600°F showed a mix between large non-equiaxed grains and columnar dendrites in their cross sections and smaller non-equiaxed grains seen in their respective longitudinal section.

Table VI. Comparative Microstructures of All Modified Casting Parameters Combinations

Mold Temp \ Pour Temp	2500°F		2600°F	
2000°F	 S1	 S2	 S3	 S4
	 S5	 S6	 S7	 S8
2100°F	 S9	 S10	 S11	 S12
	 S13	 S14	 S15	 S16

3.4 Statistical Results

Statistical analysis was conducted to quantify the meaningful difference in the output variables of grain diameter and stress rupture elongation. The two groups considered were standard casting parameters (mold temp = 1900°F, pour temp = 2800°F), and changed casting parameters. The changed casting parameters were treated as an entire group despite have differences because the

temperatures were decreased by a significant amount (200°F) and were 100°F different from each other. Additionally, there were only two possible samples from each temperature group which would make comparisons to each other less meaningful than treating all of the changed parameters as a single group. The mean and standard deviation for both parameters of rupture elongation and grain diameter for the groups of standard casting temperatures and changed temperatures are shown in Table VII.

Table VII. Mean and Standard Deviation of Stress Rupture Elongation and Grain Size

		Stress Rupture Elongation (%)	Average Grain Diameter (10 ⁻³ inches)
Standard Casting Procedures	Mean	5.75	21.18
	Std Dev	1.05	3.68
Changed Casting Procedures	Mean	5.91	14.02
	Std Dev	0.575	2.51

It can be seen that the grain diameter for the changed casting procedure group are slightly lower than the standard casting procedure, with a smaller standard deviation. The stress rupture elongation for the new parameter group increased slightly, and also had a smaller standard deviation. Despite being poured at different temperatures, the changed parameter group has less variance for both stress rupture elongation and grain diameter than the group cast at identical temperatures.

3.4.1 Test for Normality Using a Normal Probability Plot

To perform analysis on the distributions of stress rupture elongation and grain diameter, equal variance within groups and relative normality had to be proven. Equal variance was assumed since the sample sizes were close to the same size, 7 for the standard parameters and 8 for the changed parameters. To prove relative normality, a normal probability plot was used to compare the z score of each datapoint to a linear regression line. Figure 17 shows the regression plots for PCC’s standard casting parameters while Figure 18 shows the data for the changed casting parameters.

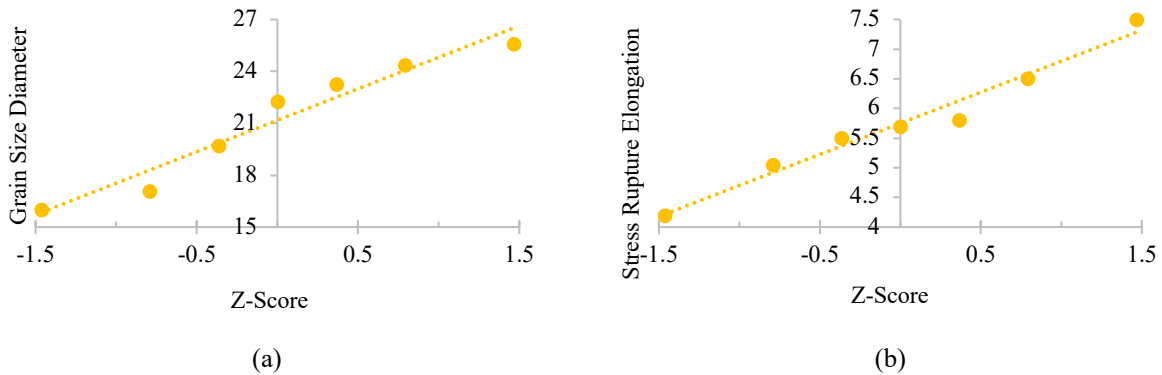


Figure 17. The average grain diameter (a) and stress rupture elongation (b) of each standard casting parameter datapoint was plotted alongside the relative z-scores and compared to a linear regression.

It can be seen that the plots dip in a predictable fashion, but not significantly enough to conclude that the distributions are two tailed. The noticeable deviations from the regression line indicate that the distribution has short tails, indicating less variance than expected in a typical normal distribution. However, all plots pass the test for relative normality, allowing for meaningful statistical analysis.

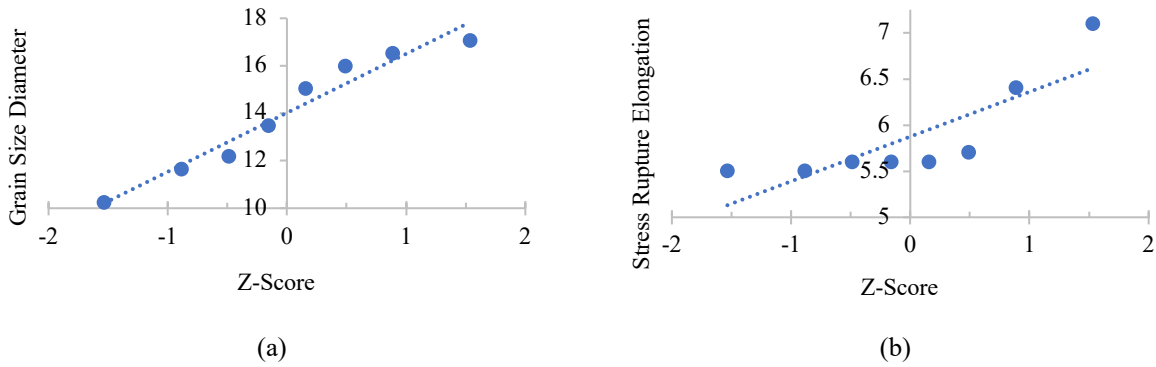


Figure 18. The average grain diameter (a) and stress rupture elongation (b) of each changed casting parameter datapoint was plotted alongside the relative z-scores and compared to a linear regression.

3.4.2 Two-Tailed T-test

The two groups being compared are standard and changed casting temperatures, meaning that a t-test is appropriate for comparison since the population mean and standard deviation are unknown. The results from the two tailed t-test are displayed below (Table VIII).

Table VIII. Outputs from T-Test Comparing Standard and Modified Casting Procedures

Parameter	P-value
Mean grain diameter	.00065
Stress rupture elongation	.775

With a P-value of .00065, it can be concluded that there is a significant difference in grain diameter between the two groups of standard and changed casting procedures. The stress rupture elongation t-test P-value of .775 is not less than .05, which does not allow for any conclusive statements about differences between the two groups.

4. Discussion

4.1 Microstructural Analysis

Microstructural changes due to the modified casting parameters show positive progress toward achieving an equiaxed polycrystalline microstructure. Although the samples with a pour temperature of 2500°F did not produce a fully equiaxed throughout the specimen, the start of an equiaxed chill zone was visible on the outer edge of the samples. Large columnar dendrites still made up the bulk of the cross section of certain samples. The lack of a fully equiaxed structure indicates that the thermal gradient between the pour and mold temperatures was still too high to allow for favorable nucleation of the ideal grain size and structure. The difference in grain shape between the cross section of samples 3 and 4 with a thermal gradient of 600°F and the cross section of samples 5 and 6 with a thermal gradient of 400°F show a noticeable shift to equiaxed grain formation (Table V). Samples 5 and 6 show large non-equiaxed grains in the center of the cross section rather than columnar dendrites. Considering PCC's concern to have consistent fill in the test bars, the pour temperature of 2500°F can be used in combination with a higher pre-heat mold temperature to reduce the thermal gradient further and decrease the cooling rate of the test bars. The decreased cooling rate should allow the equiaxed grains to nucleate and potentially limit the supercooling that occurs from high pour temperature contacting the cooler pre-heated mold.

The reduction of the average grain size and the decreased spread of the grain size data also indicated the modified casting parameters may have limited the lack-of-fusion defects that occurred in the original samples. The large columnar dendritic grains imply random concentrations of lack-of-fusion defects or shrinkage pores formed as the test bars cooled. These shrinkage pores are produced by the secondary and tertiary dendrite arms contracting during cooling, leaving small pores as potential crack nucleation sites (Figure 19).

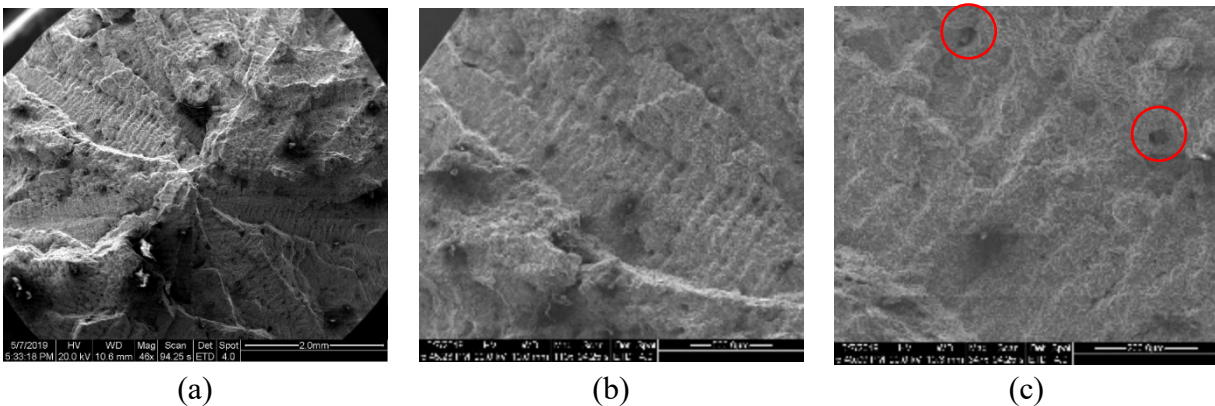


Figure 19. Scanning electron images of the stress rupture fracture surface of ML 0007359. (a) Superficial fracture surface at 46x. (b) Large columnar dendrite impression at 110x. (c) Shrinkage pores within the dendrite impression circled in red at 347x.

High concentrations of these defects could have led to internal cracks propagating through the sample during stress rupture testing, leading to the moderately ductile fracture surface seen in Figure 19a.

4.2 Stress Rupture Elongation

The combination of the large columnar dendrites and shrinkage pore formation could account for the large scatter between the stress rupture data of the as-received test bars. Random concentrations of shrinkage pores can lead to test bar fracture by crack propagation rather than high temperature ductile failure typical of stress rupture testing. Thus, the reduction of grain size in the modified castings led to lower concentrations of shrinkage pores in the samples and the mobility of the grains was limited mostly due to their large size. As a result, restricted grain motion and lower defects explain the smaller variance of the stress rupture elongation of the modified test bars (Figure 20).

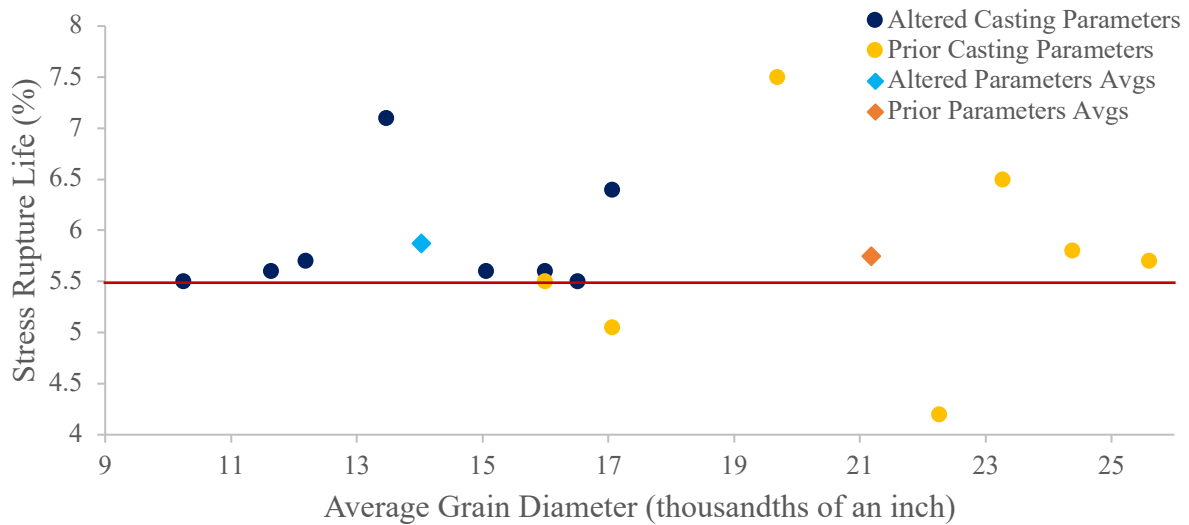


Figure 20. Stress rupture elongation and grain diameter of all specimens examined (standard and changed casting parameters).

5. Conclusions

1. All of the specimens manufactured with the modified casting parameters met or exceeded the stress rupture elongation minimum of 5.5%.
2. The modified casting parameters resulted in a statistically significant reduction in average grain diameter from .21 to .14 thousandths of an inch.
3. The modified casting parameters did not result in a statistically significant change in stress rupture elongation in the test samples.

References

- [1] Turbine Market Place. (2015, April 08). High Pressure Nozzle Guide Vanes. Retrieved from <http://www.turbinemarketplace.com/home/detail/212>
- [2] Pollock, T. M., & Tin, S. (2006). Nickel-Based Superalloys for Advanced Turbine Engines: Chemistry, Microstructure and Properties. *Journal of Propulsion and Power*, 22(2), 361-374. doi:10.2514/1.18239
- [3] Shaikh, Abdul Shaafi. (2018). Development of a γ' Precipitation Hardening Ni-Based Superalloy for Additive Manufacturing. 10.13140/RG.2.2.11472.81921.
- [4] Huang, H., & Koo, C. (2004). Characteristics and Mechanical Properties of Polycrystalline CM 247 LC Superalloy Casting. *Materials Transactions*, 45(2), 562-568. doi:10.2320/matertrans.45.562
- [5] Prasad, R. (2012). Progress in Investment Castings. *Science and Technology of Casting Processes*. doi:10.5772/50550
- [6] Reed, R. C. (2006). *The Superalloys: Fundamentals and Applications*.
- [7] ASTM E139-11(2018), Standard Test Methods for Conducting Creep, Creep-Rupture, and Stress-Rupture Tests of Metallic Materials, ASTM International, West Conshohocken, PA, 2018.
- [8] Hobbs, R., Tin, S., Rae, C., Broomfield, R., & Humphreys, C. (2004). Solidification Characteristics of Advanced Nickel-Based Single Crystal Superalloys. *Superalloys 2004 (Tenth International Symposium)*, 819-825. doi:10.7449/2004/superalloys_2004_819_825
- [9] Bhaduri, A. (2018). *Mechanical Properties and Working of Metals and Alloys*. Singapore: Springer Nature Singapore Pte Ltd. doi:10.1007/978-981-10-7209-3
- [10] Klopp, W.D. (1985). *ASM Handbook Non-Ferrous Alloys: B-1900*. Purdue Research Foundation, West Lafayette, Indiana.
- [11] ASTM E112-13, Standard Test Methods for Determining Average Grain Size, ASTM International, West Conshohocken, PA, 2013, www.astm.org